Dynamic and electronic properties of $Ce@C_{80}$: Comparative studies by the time-differential perturbed angular correlation technique with ^{140}Ce ($\leftarrow ^{140}La$) probes in graphite and diamond

Wataru Sato,* Keisuke Sueki, Yohji Achiba, and Hiromichi Nakahara
Graduate School of Science, Tokyo Metropolitan University, Hachioji, Tokyo 192-0397, Japan

Yoshitaka Ohkubo
Research Reactor Institute, Kyoto University, Kumatori, Osaka 590-0494, Japan

Kichizo Asai
Department of Applied Physics and Chemistry, The University of Electro-Communications, Chofu, Tokyo 182-8585, Japan
(Received 20 June 2000; published 13 December 2000)

Dynamic and electronic properties of $Ce@C_{80}$ as a β^- decay product of $^{140}La@C_{80}$ were investigated by means of time-differential perturbed angular correlation measurements with ^{140}Ce as the probe. Thermal motion of solid state $Ce@C_{80}$ with the activation energy of $3.7 \pm 2.3\,kJ\,mol^{-1}$ was observed at high temperature. Below the freezing temperature of the molecular motion at around 142 K, intramolecular motion of the encaged Ce atom was still observed. Dynamics of endohedral Ce fullerenes are discussed in comparison with previously reported data on $Ce@C_{82}$ and $CeLa@C_{80}$. Regarding electronic property of the encaged Ce, comparative studies with the same probes implanted in graphite and diamonds evidently suggest that encaged Ce atoms in fullerene cages possess a $4f$ electron taking the state of Ce^{3+} after β^- particle emission from the excited ^{140}La nuclei.

DOI: 10.1103/PhysRevB.63.024405 PACS number(s): 61.48.+c, 36.40.Sx, 76.80.+y

I. INTRODUCTION

Investigation on endohedral metallofullerenes has made rapid progress for the past several years, and part of the nature has gradually been unveiled by means of a wide variety of spectroscopic and electrochemical techniques.[1] Especially for mono- and dimetallofullerenes, represented by $La@C_{82}$ and $La_2@C_{80}$, dynamic and electronic properties have extensively been discussed based on various experimental observations, and intrinsic physical quantities have been obtained for some of the species.[2] However, metallofullerene studies, especially those on solid state physics, are still restricted compared with hollow fullerenes because of the limited production yield of the species.

Under this restricted circumstance, we succeeded in determining some physical quantities on the molecular and intramolecular dynamics of solid state $Ce@C_{82}$ and $CeLa@C_{80}$, β^- decay products of $^{140}La@C_{82}$ and $^{140}La^{139}La@C_{80}$ produced by the $^{139}La(n,\gamma)^{140}La$ reaction, by the time-differential perturbed angular correlation (TDPAC) method.[3,4] We adopted this method for those studies because it can provide direct information concerning the fluctuation of the principal axis of the electric field gradient (EFG) produced at the site of the probe nucleus. In other words, this method possibly allows evaluating the magnitude of the EFG and/or the reorientational correlation time of the probe nucleus perturbed by the interaction with the extranuclear field. In terms of the possibility of the simultaneous observation of static and dynamic interactions, this method has been found exceedingly suited for solid state metallofullerene studies.

In the present work, we have again applied the TDPAC technique to the study of a novel metallofullerene, $La@C_{80}$, that we recently succeeded in the isolation in a milligram quantity, and part of the dynamic and electronic properties of $Ce@C_{80}$, as a β^- decay product of $^{140}La@C_{80}$, has been revealed for the first time. For better understanding of the solid state physics of endohedral Ce fullerenes, this paper further probes into the dynamic and electronic properties by comparative studies with the same probes in different surroundings. As regards the metallofullerene dynamics, molecular and intramolecular motions of the three solid-state Ce fullerenes—$Ce@C_{82}$, $CeLa@C_{80}$, and $Ce@C_{80}$—are discussed based on some physical quantities observed for each of the molecules. Concerning the electronic states of the Ce fullerenes, the observed values for the EFGs at the encaged ^{140}Ce nuclei underwent other comparative examinations with some inorganic substances. As part of this comparative study, a nuclear fission product ^{140}Cs, which disintegrates into ^{140}Ce through a β^--decay process, was introduced in other carbon allotropes—a highly ordered pyrolytic graphite (HOPG) and granular diamonds—by the ion implantation method. Based on the comparable and/or contrastive observations, the present paper gives an interpretation to the large EFG values at the probes inside the carbon cages.

II. EXPERIMENTS

A. $Ce@C_{80}$

1. Sample production

Lanthanum-carbon composite rods were used for macroscopic production of $La@C_{80}$ as the precursor of $Ce@C_{80}$. The conventional method of arc discharge in the dc mode was employed using the carbon rods as the cathode electrode. The He gas was kept flowing in the discharge chamber under the atmospheric pressure of 150 Torr, and the dis-

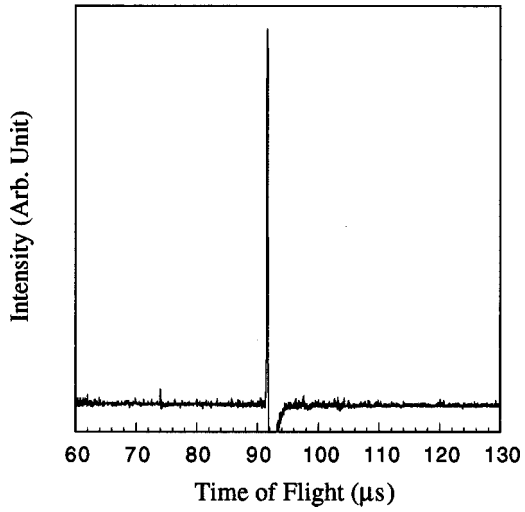

FIG. 1. LD-TOF mass spectrum of La@C_{80} isolated by the three-stage chromatographic purification.

charge current and voltage were fixed during the discharge at around 250 A and 30 to 40 V, respectively. Approximately 1 kg of carbon soot containing endohedral La fullerenes was generated in total. The soot was refluxed in 1,2,4-trichlorobenzene under a nitrogen atmosphere for the extraction of fullerene mixture. The crude extract weighed approximately 12 g after the evaporation of the 1,2,4-trichlorobenzene solvent.

For the isolation of La@C_{80}, a three-stage HPLC purification was carried out using a buckyprep column and a 5PBB column by turns with toluene eluent. A recycling-chromatography technique was employed for the third-stage purification. The isolated fraction was ascertained to be genuine La@C_{80} by laser-desorption time-of-flight (LD-TOF) mass spectrometry as shown in Fig. 1.

2. Source preparation

About 1 mg of the purified powder La@C_{80} was heat-sealed in a quartz tube together with 4 mg of powder C_{60}, which was co-sealed so that the La@C_{80} could be recovered from the tube as much as possible afterwards. The sample underwent thermal neutron irradiations at research reactors. The neutron irradiations were performed for 10 to 28 h, depending on the quantity of the sample, with the neutron fluence rate of $1.0\times10^{14}\,\mathrm{cm^{-2}\,s^{-1}}$ at JRR-3M of Japan Atomic Energy Research Institute (JAERI) and of $8.2\times10^{13}\,\mathrm{cm^{-2}\,s^{-1}}$ at Kyoto University Reactor (KUR) of Research Reactor Institute, Kyoto University. After the irradiation, the radioactive sample was recovered from the quartz tube by dissolving it in a CS_2 solvent with supersonic waves. Because there should be impurities produced by hot atom effects and/or radiation effects during the neutron irradiation, an HPLC purification with a radiochromatography technique was performed on a buckyprep column ($10\,\mathrm{mm}\,\phi\times250\,\mathrm{mm}$; Cosmosil, Nacalai Tesque Inc.) with toluene eluent at the flow rate of $3.2\,\mathrm{mL\,min^{-1}}$. The elution profile monitored with a NaI(Tl) scintillation counter is shown in Fig. 2. Recovering the eluate of interest, the powder La@C_{80} sample was finally prepared for TDPAC measurements.

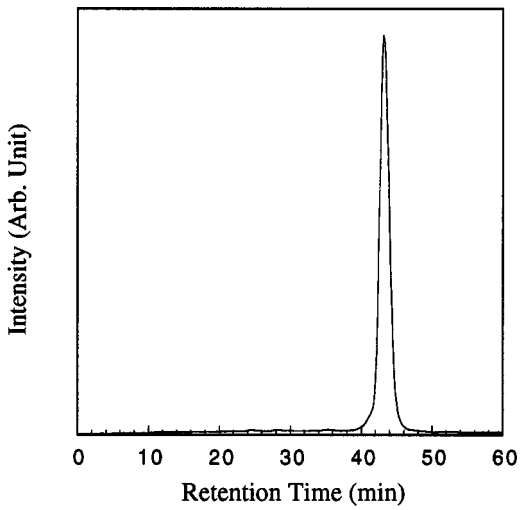

FIG. 2. HPLC radiochromatogram of radioactive La@C_{80} on a buckyprep column with toluene eluent. The elution was monitored by a NaI(Tl) scintillation counter.

3. TDPAC measurements

In the present work, the directional anisotropy of the angular correlations of the cascade γ rays was observed at $\pi/2$ and π directions with a conventional four-detector system. For the coincidence detection, BaF_2 scintillation counters with $1.5\,\mathrm{in.}\,\phi\times1\,\mathrm{in.}$ pure crystal were adopted; the time resolution of the present system was estimated to be 300 to 400 ps based on the full width at half maximum of peaks for prompt coincidence. As regards solid angle correction for the γ-ray detection, this work followed a method developed by Lawson *et al.*[5]

The TDPAC measurements were performed at various temperatures (673, 573, 473, 373, 298, 160, 100, 77, 10, and 4 K) for solid Ce@C_{80} on the (329–487)-keV cascade γ rays from ^{140}Ce nucleus, whose 2083-keV intermediate state with its nuclear spin and parity of 4^+ has a half life of 3.45 ns as shown in Fig. 3. For low-temperature measurements, the source in an aluminum tube was attached to the cold head of a cryostat equipped with a temperature controller. On the measurement at the higher temperatures than 298 K, the powder sample was heat-sealed in a pyrex glass tube in vacuum. Since there was a possibility that the metallofullerene would be deteriorated by some undesirable reaction in the process of heating up to 673 K, a TDPAC measurement was performed again after cooling down to room temperature for the purpose of the confirmation of the reproducibility of the data.

B. ^{140}Ce in other substances

1. Inorganic compounds—$PbTiO_3$ and La_2O_3

Lead titanate, $PbTiO_3$, containing La atoms as impurities was prepared following the procedure taken by Herzog *et al.*[6] A minute quantity of La_2O_3 was thoroughly mixed with stoichiometric mixture of PbO_2–TiO_2. The mixture was pressed into a disk and sintered at 800 °C for 3 h for producing La-containing $PbTiO_3$. After neutron irradiation, the

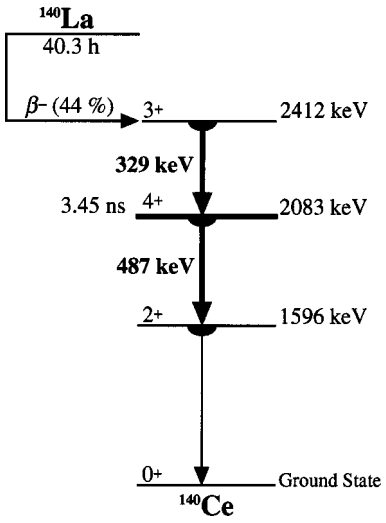

FIG. 3. Simplified decay scheme of ^{140}Ce.

sample was mixed with a macroscopic quantity of $PbTiO_3$, and annealed at 800 °C for 3 h. It is considered that the La atoms take the site of Pb in $PbTiO_3$.[6]

Powder lanthanum oxide La_2O_3 was also irradiated with reactor neutrons. The radioactive sample was then mixed with a macroscopic quantity of La_2O_3, and annealed at 1000 °C for 2 h. The x-ray powder diffraction analysis for an annealed nonradioactive La_2O_3 showed that the sample takes a hexagonal crystal system. TDPAC measurements were performed at 298 K on the (329–487)-keV cascade of ^{140}Ce for both of the samples.

2. Carbon allotropes—HOPG and granular diamonds

A highly ordered pyrolytic graphite (HOPG) NMK-1, Newmet Koch, with a size of approximately 5 mm $\phi \times 0.5$ mm was stuck on a Teflon-sheet backing of $1\times10\times10\,\mathrm{mm}^3$, and it was attached to the ion beam collector equipped at the isotope separator on-line installed at the target chamber (T-1) in KUR (KUR-ISOL). The fission products derived from the concentrated ^{235}U target in the chamber were rapidly transported into the ion source equipped outside the reactor. After surface ionization, they were accelerated by the acceleration voltage up to 30 kV and were separated according to their charge-to-mass ratios by the analyzer magnet. The ion beam of interest, ^{140}Cs, was again accelerated by the acceleration voltage of 80 kV and kept bombarded into the target HOPG for 51 h. Detailed description and a schematic diagram of the system of KUR-ISOL appear in Ref. 7 and references cited therein. The probe nucleus ^{140}Ce is formed through the following disintegration process:

$$^{140}\mathrm{Cs} \xrightarrow[63.7s]{\beta^-} {}^{140}\mathrm{Ba} \xrightarrow[12.8d]{\beta^-} {}^{140}\mathrm{La} \xrightarrow[40.3h]{\beta^-} {}^{140}\mathrm{Ce}.$$

The radioactivity of the HOPG was measured 4 days after the irradiation. It was confirmed by the γ-ray spectrum that the projectiles were well discriminated in the mass separation process. The radioactivity for ^{140}La was estimated to be 2.2×10^5 Bq. After the radioactivity of ^{140}La was fully built up, TDPAC measurements were carried out on the cascade of 329–487 keV at 298 and 10 K. Previous to the measurements, the single crystal HOPG was shredded into pieces so that the measurements were substantially performed for a polycrystalline sample.

Granular natural diamonds from DeBeers with sizes of approximately 0.5 mm ϕ were prepared as the second carbon matrix for the implantation of ^{140}Cs. All the experimental procedure and condition before the TDPAC measurements were almost the same as those for the HOPG sample. The ionized fission products were totally accelerated up to 140 kV for this run. The radioactivity for the ^{140}La implanted in the diamond grains was 5.0×10^4 Bq. The TDPAC measurements were finally performed on the same condition as those for the HOPG sample.

III. THEORETICAL DESCRIPTION

Although a basic theory of the TDPAC method has already been described in one of our previous papers,[4] a simple explanation for it is here provided again because it is considered that the equations below are requisite for better understanding of the data analyses in the present work.

For the case that the directional anisotropy of the angular correlation between the cascade γ rays is perturbed by randomly oriented extranuclear field while the probe nucleus is staying at the intermediate state of the cascade and that the circular polarization is not observed for the measurements, the directional correlation function, $W(\theta,t)$, is described by

$$W(\theta,t)=1+A_{22}G_{22}(t)P_2(\cos\theta), \tag{1}$$

if higher terms than the second order are negligibly small. Here, θ is the angle between the directions of the cascade γ rays, t is the time interval between the cascade, and A_{22} and $G_{22}(t)$ are the correlation coefficient and the time-differential perturbation factor, respectively, for the second term of the Legendre polynomials, $P_2(\cos\theta)$. The correlation coefficient A_{22} is characteristic of the multipolarities of the cascade γ rays and the nuclear spins of levels relevant to the cascade transitions. For the present case, the correlation coefficient is estimated to be -0.14 by theoretical computations by assuming pure multipole radiation.[8]

In the limited case for an axially symmetric EFG produced at the probe by the outer surrounding charge distribution, the static time-differential perturbation factor $G_{22}^{\mathrm{static}}(t)$ for the present case of $I=4$ is explicitly expressed as

$$\begin{aligned}G_{22}^{\mathrm{static}}(t)=\frac{1}{1155}[&331+10\cos(3\omega_Q t)+81\cos(9\omega_Q t)\\&+180\cos(12\omega_Q t)+175\cos(15\omega_Q t)\\&+196\cos(21\omega_Q t)+126\cos(24\omega_Q t)\\&+56\cos(36\omega_Q t)],\end{aligned} \tag{2}$$

where ω_Q represents the nuclear quadrupole frequency at the intermediate state under the EFG.

In case that the fluctuation of the extranuclear field is fast enough to prevent the probe nucleus from keeping the electrostatic interaction, another treatment on $G_{22}(t)$ has been proposed for the dynamic perturbation. When the correlation time, τ_c, for the reorientation of the principal axis of the EFG is sufficiently shorter than $1/\omega_Q$, according to the diffusion approximation deduced by Abragam and Pound,[9] the directional anisotropy shows exponential-type attenuation following the equation:

$$G_{22}^{\text{dynamic}}(t)=\exp(-\lambda t). \tag{3}$$

Here, λ is the relaxation constant, which is written in the following form in the case of the electric quadrupole interaction:

$$\lambda=\frac{3}{80}\left(\frac{eQ}{\hbar}\right)^2\left\langle\left(\frac{\partial^2 V}{\partial z'^2}\right)^2\right\rangle_{A\nu} \times\tau_c\frac{k(k+1)[4I(I+1)-k(k+1)-1]}{I^2(2I-1)^2}, \tag{4}$$

where e is the elementary electric charge, Q is the quadrupole moment of the intermediate state, $\hbar$ is Planck constant, $\langle(\partial^2 V/\partial z'^2)^2\rangle_{A\nu}$ is the ensemble average of the largest EFG in coordinates moving with the fluctuation. For the present study, $k=2$ and $I=4$.

When a four-detector system is employed for observing coincident events at the angles $\pi/2$ and π radians, the time-variant directional anisotropy, $A_{22}G_{22}(t)$, is given by a simple arithmetic operation as

$$A_{22}G_{22}(t)=\frac{2[N(\pi,t)-N(\pi/2,t)]}{N(\pi,t)+2N(\pi/2,t)}. \tag{5}$$

Here, $N(\theta,t)$ $[\propto W(\theta,t)\exp(-t/\tau_N)$, where τ_N is the mean life of the intermediate state ($=5.0$ ns for the relevant cascade)] is the number of the coincident events observed at an angle, θ.

IV. RESULTS AND DATA ANALYSIS

A. Experimental value for the correlation coefficient

The angular correlation coefficient A_{22} is theoretically evaluated to be -0.14 for the relevant cascade transition. As regards empirical estimates, there have been several papers reporting the experimental values;[10–15] however, those values vary in a quite large range (-0.097 to -0.132) possibly because of the difference of the condition of the radiation detection systems. It is therefore essential to estimate an original value for the correlation coefficient applicable for the system used in the present work.

In order to obtain the A_{22} value for this work, a TDPAC measurement for Ce ions solvated in a solution was carried out. Approximately 1.6 mg of powder La_2O_3 was irradiated with reactor neutrons for 10 min at F ring of the research reactor TRIGA II at Institute for Atomic Energy, Rikkyo University, with the thermal neutron fluence rate of $1.5\times10^{12}\,\text{cm}^{-2}\,\text{s}^{-1}$. Following the irradiation, the powder sample was dissolved in an aqueous solution of 0.1 mol L^{-1} nitric acid. After the sample was thoroughly dissolved, TDPAC measurements were performed at room temperature. The measurements were run four times on the same condition so as to obtain the average value for the relevant A_{22}. The averaged directional anisotropy $A_{22}G_{22}(t)$ as a function of the elapsing time at the intermediate state is shown in Fig. 4. The anisotropy appears constant as theoretically understood. From this observation, the experimental A_{22} for the present system was determined to be -0.125 ± 0.007, and this value will be used for data analyses hereafter.

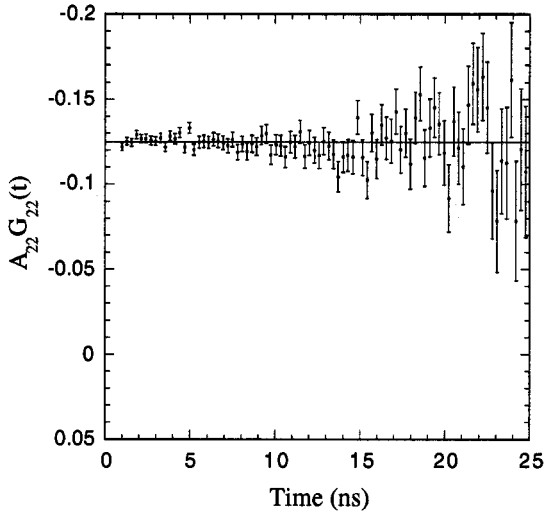

FIG. 4. TDPAC spectrum of ^{140}Ce in an aqueous solution of 0.1 mol L^{-1} nitric acid at room temperature. It was fitted by the method of least squares assuming no perturbation.

B. Ce@C_{80}

TDPAC spectra for the powder ^{140}Ce($\leftarrow{}^{140}$La)@C_{80} observed at various temperatures are shown in Fig. 5.

Taking a survey of each high-temperature spectrum, one can see that the directional anisotropies at the temperature range between 573 and 298 K show exponential-type attenuation seemingly following Eq. (3), which is a similar trend to those observed for high-temperature Ce@C_{82} and CeLa@C_{80}.[3,4] However, they do not seem to reach zero asymptotically even after a considerably long time interval between the cascade. As in the case for Ce@C_{82} and CeLa@C_{80}, the assumption that there are two different components in the perturbation functions, hence, would reasonably be allowed for Ce@C_{80}: one showing fast relaxation of the directional anisotropy and the other showing slow relaxation. Taking these two different species into consideration, accordingly, the high-temperature spectra were analyzed by least-squares fits with the following equation:

$$A_{22}G_{22}(t)=-0.125[P\exp(-\lambda_1 t)+(1-P)\exp(-\lambda_2 t)], \tag{6}$$

except for the one observed at 673 K. Here, P is the proportion of the first species, and the subscript numbers 1 and 2 stand for the first and second species. The numerical A_{22}

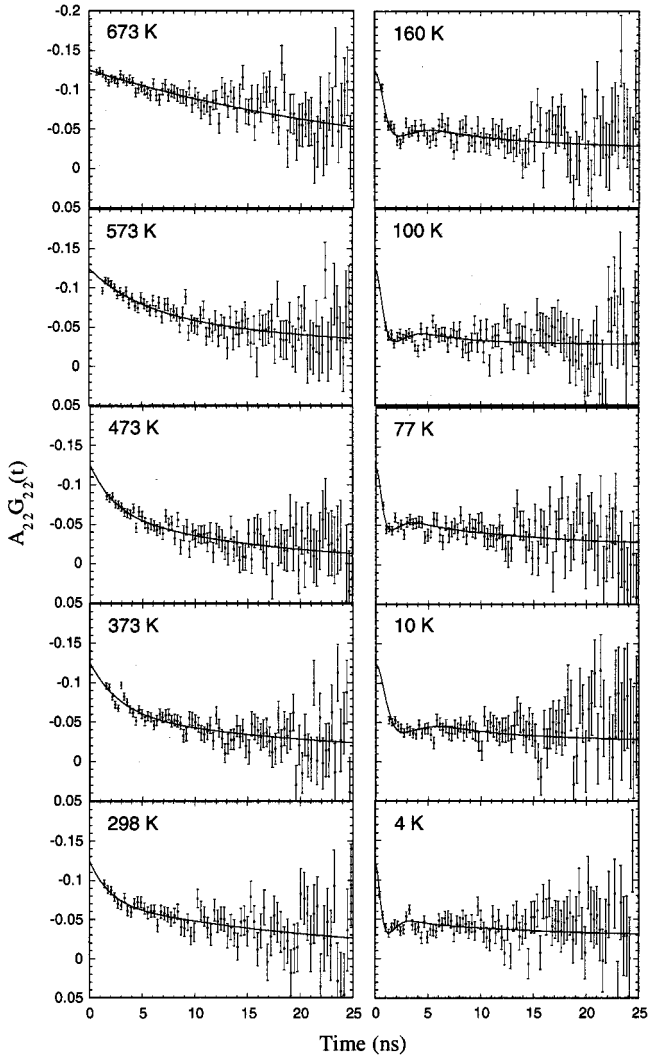

FIG. 5. TDPAC spectra of ^{140}Ce in solid Ce@C_{80} at various temperatures. Each spectrum at the high temperatures (298 to 573 K) and the low temperatures (4 to 160 K) was fitted by the method of least squares with Eqs. (6) and (7), respectively. The spectrum at 673 K was fitted with Eq. (10) assuming the presence of only one component.

$(=-0.125)$ was employed for all the data analysis. (The reason for the exclusion of the 673-K data is stated later.)

As for the low temperatures, a damped oscillatory structure can be seen in each of the spectra, which is considered to be a reflection of the nuclear spin precession caused by a static electric quadrupole interaction with the extranuclear charge distribution. The coexistence of two components admitted for the high-temperature spectra can also be assumed for those observed at the low temperatures because the first dip of the anisotropy at around 2 ns does not reach zero in spite of the intrinsic property of $G_{22}^{\text{static}}(t)$, and because the slow relaxation of the directional anisotropy observed at the high temperatures is seen in the spectra. Based on these observations, two-component fits were also applied to the analyses of those TDPAC spectra taken at 160, 100, 77, 10, and 4 K, presuming the presence of the second component showing slow exponential relaxation. The least-squares fits were accordingly carried out with

$$A_{22}G_{22}(t) = -0.125[PG_{22}^{\text{static}}(t)_{\delta\omega_Q} + (1-P)\exp(-\lambda_2 t)], \tag{7}$$

where

$$G_{22}^{\text{static}}(t)_{\delta\omega_Q} = a_0 + \sum_{i=1}^{7} a_i \exp\left(-\frac{1}{2}\delta^2\omega_{Qi}^2 t^2\right)\cos\omega_{Qi}t, \tag{8}$$

where Eq. (2) is expressed in a general form as

$$G_{22}^{\text{static}}(t) = a_0 + \sum_{i=1}^{7} a_i \cos\omega_{Qi}t. \tag{9}$$

The relative width, δ, is defined by $\delta=\sigma/\omega_Q^0$, where σ is the width of the distribution and ω_Q^0 is the centroid of ω_Q for each term.

Although the two-component analysis with the least squares was also essayed for the TDPAC spectrum observed at 673 K, the time-dependent directional anisotropy, by any means, could not be fitted well by Eq. (6). Because the directional anisotropy seems gradually attenuating in accordance with the diffusion approximation, however, it was simply reproduced on the assumption of one component by

$$A_{22}G_{22}(t) = -0.125\exp(-\lambda t). \tag{10}$$

The fitted lines by Eqs. (6), (7), and (10) are shown in each of the spectra in Fig. 5.

C. ^{140}Ce in other substances

1. Inorganic compounds—$PbTiO_3$ and La_2O_3

The TDPAC spectra of ^{140}Ce in $PbTiO_3$ and in La_2O_3 are shown in Figs. 6(a) and 6(b), respectively. Each of the directional anisotropies seems to follow the cosine functions in the static perturbation factor rather than the exponential function for dynamic perturbation. The spectra in the figure were therefore fitted by least squares with Eq. (2) assuming an axially symmetric EFG. The nuclear quadrupole frequencies optimized by the least-squares fits for $PbTiO_3$ and La_2O_3 are $\omega_Q=(1.5\pm0.1)\times10^6\,\text{rad}\,\text{s}^{-1}$ and $\omega_Q=(1.2\pm0.1)\times10^6\,\text{rad}\,\text{s}^{-1}$, respectively. The ω_Q is related by

$$\omega_Q = \frac{eQ|V_{zz}|}{4I(2I-1)\hbar} \tag{11}$$

to the EFG at the site of the probe nucleus, V_{zz}. In Eq. (11), Q is the nuclear quadrupole moment of the intermediate state of the relevant cascade ($=0.35\pm0.07$ barn for the 2083-keV state of ^{140}Ce).[16] The EFG values for $PbTiO_3$ and La_2O_3 were thus calculated as $|V_{zz}|=(3.2\pm0.7)\times10^{21}\,\text{V}\,\text{m}^{-2}$ and $(2.5\pm0.5)\times10^{21}\,\text{V}\,\text{m}^{-2}$, respectively.

2. HOPG

The TDPAC spectra of ^{140}Ce($\leftarrow^{140}$La$\leftarrow^{140}$Ba$\leftarrow^{140}$Cs) implanted in the HOPG sample are shown in Fig. 7. The 10-K

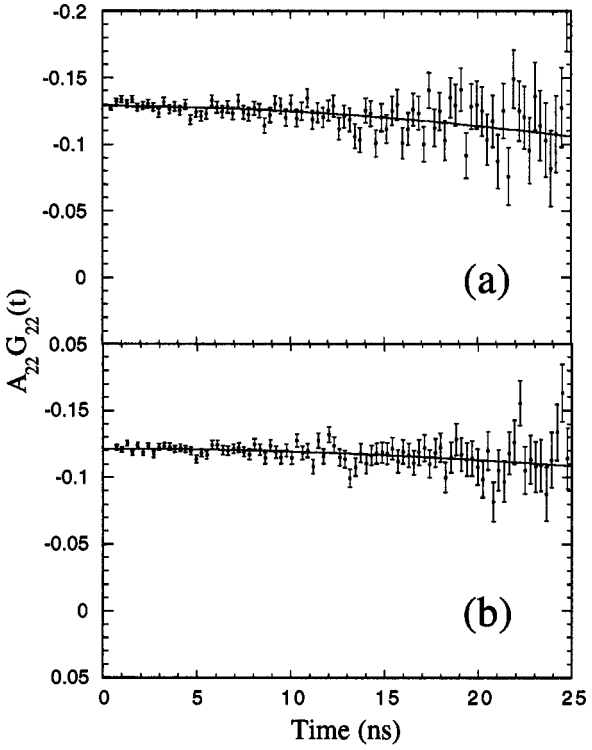

FIG. 6. TDPAC spectra of ^{140}Ce as impurities (a) in $PbTiO_3$ and (b) in La_2O_3 at 298 K. They were fitted by assuming electrostatic perturbation.

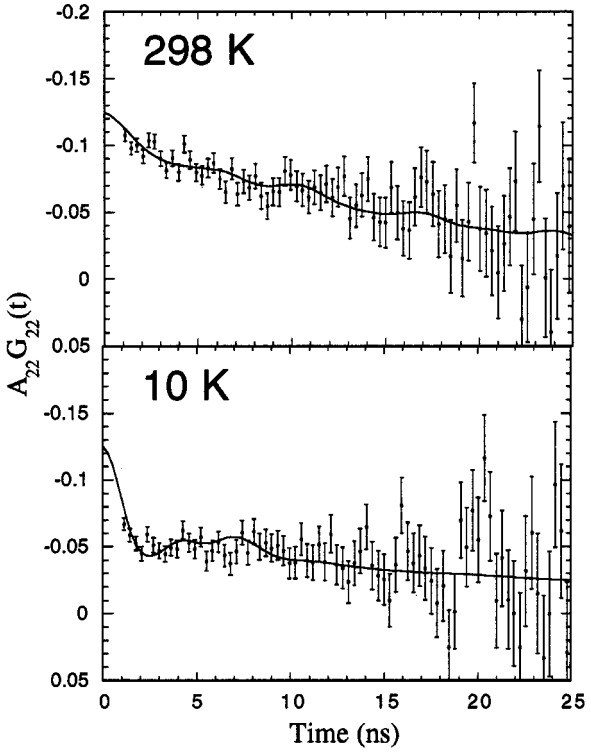

FIG. 7. TDPAC spectra of ^{140}Ce implanted in HOPG at 298 and 10 K. Both were fitted with Eq. (12).

spectrum seemingly behaves in a similar way to those for Ce@C_{80} at low temperature, which has a slowly relaxing oscillatory structure. In accordance with the analytical method taken for Ce@C_{80}, the spectrum was fitted by the method of least squares with

$$A_{22}G_{22}(t) = -0.125[PG_{22}^{\text{static}}(t)_{\delta\omega_Q} + (1-P)\exp(-\lambda t)]. \tag{12}$$

Here, the presence of two different components was again assumed: The first component shows a damped oscillatory structure implying an electrostatic perturbation from the extranuclear field, and the directional anisotropy for the second component exponentially attenuates suggesting a dynamic perturbation on the probe nucleus. With regard to the electric quadrupole interaction for the first component, the nuclear quadrupole frequency and the EFG estimated thereby were optimized as $\omega_Q = (7.2 \pm 0.3) \times 10^7\ \text{rad s}^{-1}$ and $|V_{zz}| = (1.5 \pm 0.3) \times 10^{23}\ \text{V m}^{-2}$, respectively.

As for the TDPAC spectrum measured at room temperature, there also appears an oscillatory structure with a small amplitude in the slowly relaxing directional anisotropy. Taking this trend into account, a least-squares fit was performed on the spectrum with Eq. (12).

3. Diamonds

The TDPAC spectra observed at 10 and 298 K for the ^{140}Ce($\leftarrow{}^{140}$La$\leftarrow{}^{140}$Ba$\leftarrow{}^{140}$Cs) implanted in the granular diamonds are shown in Fig. 8. Unlike the time-dependent behavior of the directional anisotropy for the HOPG sample, each of the spectra goes down in arc, whose trend is quite similar to those observed for ^{140}Ce in $PbTiO_3$ and La_2O_3. Following the analytical method adopted for those compounds, therefore, both of the TDPAC spectra were fitted in the same way as the inorganic compounds assuming the presence of one component. For the TDPAC spectrum at 10 K, the optimized value for the nuclear quadrupole frequency and the EFG at the probe are $\omega_Q = (2.5 \pm 0.2) \times 10^6\ \text{rad s}^{-1}$ and $|V_{zz}| = (5.3 \pm 1.1) \times 10^{-21}\ \text{V m}^{-2}$, respectively.

V. DISCUSSION

A. Ce@C_{80}

1. Molecular and intramolecular dynamics

For all the temperature range, general trend of the time variation of the directional anisotropies for Ce@C_{80} is similar to that for Ce@C_{82};[3] at high temperature, the anisotropies seem to exponentially attenuate, whereas damped oscillatory structures appear in the observed perturbation functions at low temperature range. In addition, there are also two different components in all the TDPAC spectra taken at the temperature range between 573 and 4 K.

For examining the temperature variation of the behavior of the anisotropies, the values for the relaxation constants, an index for the motional time scale, optimized by the least-squares fits are plotted as a function of reciprocal temperature in Fig. 9. In the high temperature range, the values for λ_1 and λ_2 become larger with decreasing temperature, which directly implies a thermally activated motion of the molecules. On the analogy of the interpretation made for the

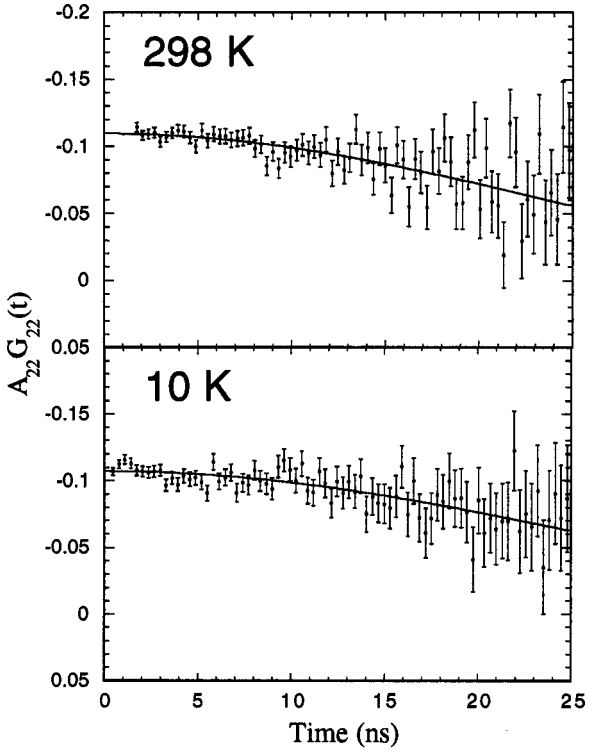

FIG. 8. TDPAC spectra of ^{140}Ce implanted in granular diamonds at 298 and 10 K. Both were fitted by assuming electrostatic perturbation.

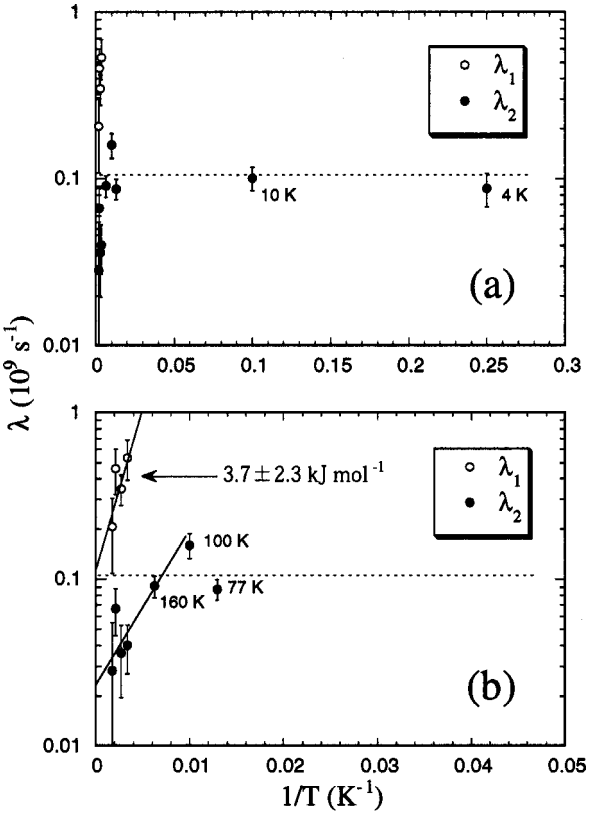

FIG. 9. (a) Temperature dependence of the relaxation constants (λ_1 and λ_2) for solid Ce@C_{80}. It is enlarged in (b) for a detailed examination of the high temperature range. The broken horizontal lines indicate the average value of λ_2 at the low temperatures.

experimental data for Ce@C_{82},[3] the abrupt change of the temperature dependence at around 142 K, observed for λ_2, can be attributed to the freeze of the molecular rotation on the time scale of the interval of the relevant cascade. The first component at the high temperatures makes the transition to the one showing the oscillatory structure in the low-temperature spectra, and the slowly relaxing second component to the other; this correspondence is ascertained by the invariance of the P values above and below the temperature of the presumed freeze of the molecular rotation and by the smooth continuity of the λ_2 values around this freezing point.

Even below the freezing temperature, it is obvious that the directional anisotropies for the second component show slow relaxation, implying some dynamic perturbation acting on the probe nucleus. Because the molecular motion is presumed to be freezing below 142 K, it is the intramolecular dynamic motion of the encaged atom that is the most conceivable mode of the motion associated with the dynamic perturbation. The recoil effect triggered by the β^- particle emission from the parent nuclide ^{140}La would be nominated for the driving force of the intramolecular motion since there is little, if any, temperature dependence on the observed λ_2 values. Because the directional anisotropies for the second component are slowly relaxing, it is considered that the probe atom is enabled to make a motion, lasting for at least the time scale of nanoseconds, in the hollow space provided by the spherically closed cage structure of C_{80}.

The average value of the proportion of the first component, $\langle P \rangle$, was estimated by the least-squares fits of the $A_{22}G_{22}(t)$ to be 0.73 ± 0.06. If the above interpretation on the intramolecular motion is accepted, the first component corresponds to the species with the encaged atom accommodated in a certain potential well on the cage, and the second component is regarded as those with the probe atom in motion inside the cage. Therefore, the above $\langle P \rangle$ value evidently shows that only 30% or less of the whole Ce@C_{80} are allowed to have the intramolecular motion of the probe atoms having received enough recoil energy to jump out of the potential well where the probes are initially accommodated.

Assuming the interpretation above, the activation energy for the molecular rotational motion was evaluated by a least-squares fit of the λ_1 values with an Arrhenius-type equation

$$\lambda_1 = A \exp\left(\frac{E_a}{RT}\right) \tag{13}$$

as $3.7 \pm 2.3\,\mathrm{kJ\,mol^{-1}}$.

The two-component analysis could not be applied to the TDPAC spectrum measured at 673 K. For understanding the spectrum, the effect of thermal agitation should be taken into account. It is inferred that at this high temperature the thermal activation is such that it makes no difference in the relaxation rate of the directional anisotropies whether the probe atom has internal motion or not as far as the present detection circuit of the limited time resolution is used. In consequence, there seems to be no longer an appreciable gap

at this high temperature between the time scales of the presumed different motions: the overall molecular rotation and the intramolecular circular motion of the probe. The sublimation temperatures for C_{60} and C_{70} have been reported to be 300 and 350 °C, respectively.[17] Although it is unknown whether the spectral change took place gradually or not since there is a gap in temperature as large as 100 K between the 673 and 573 K, the possibility of such a phase transition as the sublimation of C_{60} and C_{70} in this temperature range cannot be excluded. A further detailed investigation is needed for elucidating the solid state dynamics of Ce@C_{80} at high temperature.

2. Nuclear quadrupole interaction

As discussed in the preceding subsection, the first component in each of the TDPAC spectra observed below the freezing point of the thermal molecular rotation shows an oscillatory structure following Eq. (2), suggesting the nuclear precession of the probe arising from a static nuclear quadrupole interaction. The least-squares fits on the low temperature spectra (160, 100, 77, 10, and 4 K) with Eq. (7) yielded the optimized ω_Q values, from which their average value was estimated to be $\langle \omega_Q \rangle = (1.0 \pm 0.1) \times 10^8$ rad s^{-1}. With Eq. (11), the largest EFG on the principal axis at the site of the probe nucleus is evaluated by the substitution of the $\langle \omega_Q \rangle$ value: $|V_{zz}| = (2.1 \pm 0.4) \times 10^{23}$ V m^{-2}. This large value is further discussed later in comparison with the observed values for other substances.

B. ^{140}Ce in other substances

1. Inorganic compounds—$PbTiO_3$ and La_2O_3

The TDPAC spectra for both $PbTiO_3$ and La_2O_3 suggest that the probes have electrostatic interaction with the outer surrounding charge distribution, and it was further found that the different surroundings of the probe ^{140}Ce do not have a significant effect on the magnitude of the EFGs. This phenomenon may be explained by assuming that there is little difference in the electron distribution in the inner closed shell of the probe atoms.

2. HOPG

As shown in Fig. 7, the trend of the perturbation functions is the same on the whole as those for Ce@C_{80}. As in the case for Ce@C_{80}, therefore, the probe nucleus is plausibly interpreted as statically and dynamically perturbed by the extranuclear field as to the first and second components, respectively.

What should be noted is that the proportion of the first component denoted by P in Eq. (12) gives appreciably differing values at different temperatures: $P = 0.54 \pm 0.03$ and 0.14 ± 0.01 at 10 and 298 K, respectively. If the above interpretation is accepted here, the probe nuclei in most of the species, 86%, are considered to have dynamic motion at room temperature. The driving force of this motion at the high temperature is reasonably ascribable to thermal activation as well as the recoil energy of the β^- disintegration because the rate of the exponential decay seen in the TDPAC spectrum at 298 K is distinctly different from that for 10-K spectrum. The probe nuclei, hence, is considered to move easily and to have greater momentum at room temperature than those at 10 K resulting in such large proportion for the second component in motion. This interpretation is supported by the observed values for the relaxation constant: $\lambda = (0.092 \pm 0.009) \times 10^9$ s^{-1} and $(0.056 \pm 0.004) \times 10^9$ s^{-1} at 10 and 298 K, respectively. This observation evidently shows that the probe atom moves faster at the higher temperature. Concerning the EFG at the probe, the value is somewhat small compared with the 10-K data, which may reflect the averaging effect and the subtle change of the lattice constant owing to the rise of temperature.

3. Diamonds

It is obviously recognized from the fits that the probe ^{140}Ce nucleus in the diamonds is statically perturbed by the outer surrounding charge distribution with negligibly small temperature dependence. Since a diamond crystal has a rigid framework of sp^3 hybridization, the probes should be confined at some fixed sites in limited spaces, possibly in interstitial positions,[18] after the implantation, and thus the recoil energy of the β^- particle emission should be mostly dissipated before the first 329-keV γ-ray emission. It is hence reasonable that the observed perturbation functions show a typical static perturbation reflecting electric quadrupole interaction between the probes and the lattice, and that a dynamic perturbation such as in the case of the Ce@C_{80} and the HOPG is not seen even at room temperature.

VI. COMPARATIVE STUDIES

A. Cerium fullerene dynamics

Some physical quantities obtained in a series of our works for Ce@C_{82}, Ce@C_{80}, and CeLa@C_{80} are summarized in Table I.[19]

For the monometallofullerenes, the relaxation constant λ_1 is an appropriate index for the direct comparison of the molecular motions. The λ_1 value for Ce@C_{80} is approximately three times as large as that for Ce@C_{82} at room temperature. Although the difference cannot directly be attributed to the correlation time τ_c because the λ_1 is a function of the ensemble average for the nuclear quadrupole frequency as well, the τ_c value for Ce@C_{80} is estimated to be 40% larger than that for Ce@C_{82} even considering the difference in the average EFG values observed at low temperatures. Accordingly, it can be concluded that Ce@C_{80} has somewhat slow rotational motion at room temperature compared with Ce@C_{82} in the solid form.

The activation energy E_a for the relaxation constant λ_1 is also a significant physical quantity for discussing the solid state physics of fullerene molecules. It has been found that the E_a values do not show an appreciable difference between both of the species. This observation may suggest that the intermolecular force is almost equal to each other in the rotator phase. (This inference is based on the assumption that the ensemble averages for the EFG in coordinates moving with the fluctuation of the system for each species have equal temperature dependence for both of the species.)

TABLE I. Physical quantities for $Ce@C_{82}$, $Ce@C_{80}$, and $CeLa@C_{80}$ optimized by the least-squares fits of the TDPAC spectra.

Ce fullerenes	λ_1 $(10^9\ s^{-1})$[a]	E_a $(kJ\ mol^{-1})$	T_F (K)	$\langle\lambda_2\rangle(10^9\ s^{-1})$[b]	$\langle 1-P\rangle$
$Ce@C_{82}$	0.19 ± 0.02	4.5 ± 0.4	114	0.038 ± 0.004	0.66 ± 0.04
$Ce@C_{80}$	0.54 ± 0.14	3.7 ± 2.3	142	0.11 ± 0.03	0.27 ± 0.02
$CeLa@C_{80}$			158		0.84 ± 0.05[c]

[a]Room temperature values.

[b]Average values at the low temperatures.

[c]Average proportions for the components having intramolecular motion of the encaged atoms.

The freezing temperature of the molecular rotation T_F can also be an important clue to the elucidation of the molecular interaction. As shown in Table I, their values for the species are distinct from each other, which clearly indicates that there is a difference in the molecular interaction in the low-temperature phase between $Ce@C_{82}$ and $Ce@C_{80}$; more specifically, $Ce@C_{80}$ in the low-temperature phase needs high energy for initiating the rotational motion compared with $Ce@C_{82}$.

According to the proposed interpretation, the parameter for the low temperatures below the T_F is associated only with intramolecular dynamic motion of the encaged atom; this means that it is possible to provide insight into the dynamic motion separately from the molecular rotation. The difference in the average λ_2 values between $Ce@C_{82}$ and $Ce@C_{80}$ explains that the reorientational correlation time of the nuclear spin of the probes in $Ce@C_{80}$ is approximately three times as long as that for $Ce@C_{82}$, which means that the Ce atom encaged in the C_{82} cage is moving around inside the carbon cage faster than that in the C_{80} cage. (This interpretation is based on the assumption that there is no difference in the ensemble average for the EFG at the probe nuclei between $Ce@C_{82}$ and $Ce@C_{80}$ because the atoms are presumed to have jumped out of the potential leaving no rigid bonding with the cage. It is to be noted, however, that this interpretation is still valid even if the difference of the EFGs obtained for the first components is taken into account.) The slower motion of the Ce atoms in the C_{80} cage may imply that they are trapped in a rather deep potential and/or there are more potential ripples to overcome compared with the C_{82} cage, which requires them to have higher energy in order to initiate and/or maintain the intramolecular motions.

The proportions of the two different components in each TDPAC spectrum are also closely related to the intramolecular motion. As shown in Table I, the average values of the second component proportion, $\langle 1-P\rangle$, for both molecules are obviously different from each other. According to the interpretation above, the second component in the respective TDPAC spectra represents the species with the encaged atom moving around inside the cage. The larger value of the proportion for $Ce@C_{82}$ evidently denotes that the percentage of the mobile atoms encaged is greater than that for $Ce@C_{80}$. This phenomenon can plausibly be attributed to the difference in the depth of the potential well where the encaged atoms are originally accommodated; namely, the ^{140}Ce as in the C_{80} cage of $Ce@C_{80}$ is strongly bound to the wall of the cage compared with $Ce@C_{82}$. This consequence is consistent with the conclusion deduced with respect to the $\langle\lambda_2\rangle$ values. As regards $CeLa@C_{80}$, we have experimentally found that most of the species have intramolecular diatomic motion even at considerably low temperature,[4] which is consistent with the result of an NMR study reported by Akasaka *et al.*[20] Although diatomic motion is unlikely to take place compared with single-atom motion, the encaged atoms have motion rather freely, in fact, as for the dimetallofullerene. The low threshold barrier due to the perfectly spherical cage with I_h symmetry is considered to facilitate the diatomic motion in such high proportion of $\langle 1-P\rangle$.

B. Electric field gradient at ^{140}Ce nuclei

In Table II are listed the nuclear quadrupole frequency ω_Q and the principal component of the EFG for ^{140}Ce in several substances. As for the inorganic compounds, no clear distinction can be seen in the magnitudes of the EFGs considering their uncertainties, which implies that the outer lattice ions surrounding the ^{140}Ce with different configuration do not significantly affect the production of the EFG. In ordinary inorganic compounds, the valence state of the ^{140}Ce after the nuclear transformation of ^{140}La through the disintegration process $^{140}La \xrightarrow{\beta^-} {}^{140}Ce$ is reportedly tetravalent, Ce^{4+},[10–13,21] having the same electronic configuration as the atomic xenon. Since the electronic configuration of Xe has spherically symmetric structure with the fully filled atomic orbitals, the inner closed shell of $^{140}Ce^{4+}$ is also presumed to be hardly distorted. The small EFG values observed for the inorganic compounds can be rationalized by the inner closed shell structures with a spherical symmetry which is hardly deformed by the outer surrounding ions.

TABLE II. Nuclear quadrupole frequencies and the electric field gradients at the ^{140}Ce nucleus in some inorganic substances optimized by the least-squares fits of the TDPAC spectra.

Substances	$\langle\omega_Q\rangle(10^6\ rad\ s^{-1})$	$\lvert V_{zz}\rvert(10^{21}\ V\ m^{-2})$
$PbTiO_3$	1.5 ± 0.1	3.2 ± 0.7
La_2O_3	1.2 ± 0.1	2.5 ± 0.5
Diamonds	2.5 ± 0.2	5.3 ± 1.1
HOPG	72 ± 3	150 ± 30
$Ce@C_{82}$	70 ± 8	150 ± 30
$Ce@C_{80}$	100 ± 10	210 ± 40
$CeLa@C_{80}$	100 ± 10	210 ± 40

Concerning the endohedral Ce fullerenes, however, the estimated values for the principal components of the EFGs are large by one or two orders of magnitude over those for ^{140}Ce in $PbTiO_3$ and La_2O_3. Because it was found from the similar results on the inorganic compounds that the difference of the outer surrounding lattice makes little difference in the EFGs, such large EFG values for the metallofullerenes are hardly ascribable to the outer charge distribution in the quasi-π orbital of the carbon cage. We accordingly propose here that a different valence state of the ^{140}Ce be a principal factor in making the great magnitude of the EFGs. More specifically, it is inferred that the probe ^{140}Ce in the fullerene cages has an electron in its $4f$ orbital, taking the valence state of Ce^{3+}. This inference is based on the following circumstantial evidences: (1) cerium is known to exist in the nature taking trivalent chemical states as well as tetravalence, and (2) a fullerene cage is, in general, filled with π electrons delocalizing on the network of quasi-sp^2 hybridized orbital of carbons, which produce reducing atmosphere inside the cage. The observation can be explained by assuming that the $4f$ electron highly contributes to the magnitude of the EFG.

For verifying the inductive inference on the valence state of the metallofullerenes, graphite is the right material because it has the capability of donating its own π electrons delocalizing on the sp^2 carbon network. The directional anisotropies observed for the ^{140}Ce implanted in the HOPG at 10 K showed similar behavior to those for the endohedral Ce fullerenes, as expected; the values of the EFGs produced at the probe nuclei in the fullerene cages and the HOPG are in good agreement in the order of magnitude with one another. These experimental results thus strongly support the interpretation on the existence of a $4f$ electron.

Contrary to those ^{140}Ce adjacent to carbons with the sp^2 hybridization, it was found from the TDPAC measurement that ^{140}Ce in the granular diamonds is in manifestly different surroundings electronically as well as structurally. The principal component of the EFG at the site of the probe nucleus is considerably small compared with the corresponding values for the metallofullerenes and the HOPG. This experimental result may be interpreted in the same way as those for the inorganic compounds. After the disintegration process of $^{140}Ce(\leftarrow{}^{140}La\leftarrow{}^{140}Ba\leftarrow{}^{140}Cs)$, the probe ^{140}Ce is presumed to remain tetravalent, $^{140}Ce^{4+}$, because electron transfer from the lattice carbons would not take place owing to the localization of the electrons contributing to the σ bond formation. This allows the same inference made for the inorganic compounds that the absence of a $4f$ electron leads to such a small magnitude of the EFG.

VII. SUMMARY AND CONCLUSIONS

The TDPAC method has successfully revealed part of the solid state physics of $Ce@C_{80}$, a β^- decay product of $La@C_{80}$, through electric quadrupole interactions. At high temperature, thermally activated molecular motion of $Ce@C_{80}$ was observed from the temperature dependence of the TDPAC spectra. The activation energy for the motion was estimated to be $3.7\pm2.3\,\mathrm{kJ\,mol^{-1}}$, which is equal to that for $Ce@C_{82}$ within the uncertainties. The temperature dependence abruptly changes at around 142 K, implying the freeze of the molecular rotation. As for approximately 30% of the species, the dynamic perturbation was observed even below the freezing temperature, which was assigned to the intramolecular motion of the encaged atom. From the temperature independence of the motion, we have ascribed it to the recoil effect of the β^- particle emission from the excited ^{140}La precursor. The recoil-induced intramolecular motion is considered to last for at least the time scale of nanoseconds by overcoming the potential undulation produced inside the cages. This seems indeed an extraordinary phenomenon in the study of hot atom effect.

The physical quantities observed in a series of our works were compared for obtaining information on molecular and intramolecular dynamics of endohedral cerium fullerenes—$Ce@C_{82}$, $Ce@C_{80}$, and $CeLa@C_{80}$. It has been found from the optimized relaxation constants that solid state $Ce@C_{80}$ has slower motion than $Ce@C_{82}$ at room temperature. Regarding intramolecular motion, the encaged Ce atom of $Ce@C_{80}$ moves around slowly compared with $Ce@C_{82}$ if the same average values of the fluctuating EFGs are assumed. Two-component analyses of the observed TDPAC spectra for the metallofullerenes have clarified the mobility of the encaged Ce atoms; the potential well produced by the C_{80} cage for the singly encapsulated Ce atom is the deepest of the three.

Comparative studies were also performed for discussing the electronic states of the Ce fullerenes. For all the Ce fullerenes, the principal components of the EFGs at the site of the probe ^{140}Ce nuclei were estimated to be $\sim10^{23}\,\mathrm{V\,m^{-2}}$. Considering that the corresponding values for the probe ^{140}Ce incorporated in other inorganic compounds are small by one or two orders and are almost equal to each other despite the different crystal structures, we have inferred that the probe ^{140}Ce encapsulated in the fullerene cages is in the state of Ce^{3+} because the presence of a $4f$ electron can be regarded as making by far greater contribution to the EFG than the aspherical charge distribution in the outer lattice. This inference is indeed verified by the TDPAC measurements for ^{140}Ce implanted in HOPG and diamonds. The EFG value for the HOPG—with abundant π electrons—is in good agreement with those for Ce fullerenes within the uncertainties, whereas for diamonds—with π electrons deficient—the TDPAC pattern is almost the same as those for the inorganic compounds, signifying that the probe is in the tetravalent state, Ce^{4+}, in the diamonds.

Concerning endohedral Ce fullerenes with their Ce nuclei in the ground state, the encapsulated atoms have generally been regarded as trivalent through spectroscopic and electrochemical techniques.[22–24] In addition to the information, the present work have concluded that the probe Ce can also change to the low oxidation state by accepting an electron to a $4f$ orbital before the first γ-ray emission by way of the tetravalence taken immediately after the β^- decay. This phenomenon evidently suggests that these fullerenes indeed possess an extremely reducing atmosphere inside the cages.

ACKNOWLEDGMENTS

The authors are grateful for helpful advice from Professor M. Katada. They also thank Professor Y. Kawase, Dr. A. Taniguchi, and Dr. M. Tanigaki for their arrangement for the experiment and operation of KUR-ISOL. The granular diamonds were generously donated for the research by Professor A. Shinohara. W.S. would like to express his gratitude to Professor K. Asahi for his special interest in this work. The present work was accomplished as part of the Inter-University Program for the Common Use of JAERI Facilities and of the Visiting Researcher's Program of the Kyoto University Research Reactor Institute (KURRI). This work was partly supported by a grant from the Ministry of Education, Culture, Sports, and Science of Japan.

*Present address: Applied Nuclear Physics Laboratory, RIKEN (The Institute of Physical and Chemical Research), Wako, Saitama 351-0198, Japan.

[1] For example, Y. Chai, T. Guo, C. Jin, R. E. Haufler, L. P. F. Chibante, J. Fure, L. Wang, J. M. Alford, and R. E. Smalley, J. Phys. Chem. **95**, 7564 (1991); M. Takata, B. Umeda, E. Nishibori, M. Sakata, Y. Saito, M. Ohno, and H. Shinohara, Nature (London) **377**, 46 (1995); S. Stevenson, G. Rice, T. Glass, K. Harich, F. Cromer, M. R. Jordan, J. Craft, E. Hadju, R. Bible, M. M. Olmstead, K. Maitra, A. J. Fisher, A. L. Balch, and H. C. Dorn, Nature (London) **401**, 55 (1999); R. D. Johnson, M. S. de Vries, J. Salem, D. S. Bethune, and C. S. Yannoni, Nature (London) **355**, 239 (1992); S. Hino, H. Takahashi, K. Iwasaki, K. Matsumoto, T. Miyazaki, S. Hasegawa, K. Kikuchi, and Y. Achiba, Phys. Rev. Lett. **71**, 4261 (1993); T. Pichler, M. S. Golden, M. Knupfer, J. Fink, U. Kirbach, P. Kuran, and L. Dunsch, Phys. Rev. Lett. **79**, 3026 (1997).

[2] For example, M. Takata, E. Nishibori, B. Umeda, M. Sakata, E. Yamamoto, and H. Shinohara, Phys. Rev. Lett. **78**, 3330 (1997); P. Kuran, M. Krause, A. Bartle, and L. Dunsch, Chem. Phys. Lett. **292**, 580 (1998); K. Sueki, K. Akiyama, K. Kikuchi, and H. Nakahara, J. Phys. Chem. B **103**, 1390 (1999).

[3] W. Sato, K. Sueki, K. Kikuchi, K. Kobayashi, S. Suzuki, Y. Achiba, H. Nakahara, Y. Ohkubo, F. Ambe, and K. Asai, Phys. Rev. Lett. **80**, 133 (1998).

[4] W. Sato, K. Sueki, K. Kikuchi, S. Suzuki, Y. Achiba, H. Nakahara, Y. Ohkubo, K. Asai, and F. Ambe, Phys. Rev. B **58**, 10 850 (1998).

[5] J. S. Lawson, Jr. and H. Frauenfelder, Phys. Rev. **91**, 649 (1953).

[6] P. Herzog, B. Klemme, and G. Schäfer, Z. Phys. **269**, 265 (1974).

[7] Y. Kawase, K. Okano, and K. Aoki, Nucl. Instrum. Methods Phys. Res. B **26**, 341 (1987).

[8] H. Frauenfelder and R. M. Steffen, in *α-, β-, and γ-Ray Spectroscopy*, edited by K. Siegbahn (North-Holland, Amsterdam, 1974), Vol. 2, p. 1198.

[9] A. Abragam and R. V. Pound, Phys. Rev. **92**, 943 (1953).

[10] R. M. Levy and D. A. Shirley, Phys. Lett. **3**, 46 (1962).

[11] N. Kaplan, S. Ofer, and B. Rosner, Phys. Lett. **3**, 291 (1962).

[12] H. J. Körner, E. Gerdau, C. Günther, K. Auerbach, G. Mielken, G. Strube, and E. Bodenstedt, Z. Phys. **173**, 203 (1963).

[13] M. Schmorak, H. Wilson, P. Gatti, and L. Grodzins, Phys. Rev. B **134**, B718 (1964).

[14] M. E. Wiedenbeck and D. E. Raeside, Nucl. Phys. **A176**, 381 (1971).

[15] M. Mekata, Y. Kano, M. Moriya, K. Tsuji, and T. Haseda, J. Phys. Soc. Jpn. **41**, 1918 (1976).

[16] *Table of Isotopes*, 8th ed., edited by R. B. Firestone and V. S. Shirley (Wiley, New York, 1996), Vol. 1.

[17] D. M. Cox, S. Behal, M. Disco, S. M. Gorun, M. Greaney, C. S. Hsu, E. B. Kollin, J. Millar, J. Robbins, W. Robbins, R. D. Sherwood, and P. Tindall, J. Am. Chem. Soc. **113**, 2940 (1991).

[18] D. Surono, F.-J. Hambsch, and P. W. Martin, Hyperfine Interact. **96**, 23 (1995).

[19] The values for Ce@C_{82} and CeLa@C_{80} are somewhat different from those shown in Refs. 3 and 4 because those data were reanalyzed using $A_{22}=-0.125$.

[20] T. Akasaka, S. Nagase, K. Kobayashi, M. Wälchli, K. Yamamoto, H. Funasaka, M. Kako, T. Hoshino, and T. Erata, Angew. Chem. Int. Ed. Engl. **36**, 1543 (1997).

[21] B. Klemme and H. Miemczyk, J. Phys. Soc. Jpn. **34**, 265 (1973).

[22] J. Ding, L.-T. Weng, and S. Yang, J. Phys. Chem. **100**, 11 120 (1996).

[23] T. Suzuki, K. Kikuchi, F. Oguri, Y. Nakao, S. Suzuki, Y. Achiba, K. Yamamoto, H. Funasaka, and T. Takahashi, Tetrahedron **52**, 4973 (1996).

[24] J. Ding and S. Yang, Angew. Chem. Int. Ed. Engl. **35**, 2234 (1996).